Effects of spatial dispersion in near-field radiative heat transfer between two parallel metallic surfaces

Pierre-Olivier Chapuis,[1,*] Sebastian Volz,[1] Carsten Henkel,[2] Karl Joulain,[3] and Jean-Jacques Greffet[1]
[1]*Laboratoire d'Energétique Moléculaire et Macroscopique, Combustion, CNRS UPR 288, Ecole Centrale Paris, Grande Voie des Vignes, F-92295 Châtenay-Malabry Cedex, France*
[2]*Universität Potsdam, Institut für Physik, Am Neuen Palais 10, 14469 Potsdam, Germany*
[3]*Laboratoire d'Etudes Thermiques, ENSMA, 86961 Futuroscope Chasseneuil Cedex, France*
(Received 3 October 2007; published 25 January 2008)

We study the heat transfer between two parallel metallic semi-infinite media with a gap in the nanometer-scale range. We show that the near-field radiative heat flux saturates at distances smaller than the metal skin depth when using a local dielectric constant and investigate the origin of this effect. The effect of nonlocal corrections is analyzed using the Lindhard-Mermin and Boltzmann-Mermin models. We find that local and nonlocal models yield the same heat fluxes for gaps larger than 2 nm. Finally, we explain the saturation observed in a recent experiment as a manifestation of the skin depth and show that heat is mainly dissipated by eddy currents in metallic bodies.

DOI: 10.1103/PhysRevB.77.035431 PACS number(s): 78.20.Bh

I. INTRODUCTION

Near-field radiative heat transfer has been investigated for 40 years.[1–28] Rytov and coworkers[1] showed how to calculate thermal radiation by introducing fluctuational electrodynamics. This theory is based on the introduction of random current densities due to the thermal random motion of charges. Their correlation functions are given by the fluctuation-dissipation theorem. Cravalho, Tien, and Caren[2] and Olivei[3] were the first to address heat transfer in the near field, i.e., at distances smaller than the peak wavelength λ_T of the thermal radiation spectrum. However, they did not consider all evanescent waves. Polder and Van Hove[8] were the first to take into account all the evanescent waves by using the formalism introduced by Rytov. They found a huge increase in the heat flux between two parallel surfaces when the gap distance d becomes smaller than λ_T. Levin *et al.*[11] pointed out that spatial dispersion could play a role for small gaps. Volokitin and Persson[19] showed that spatial dispersion could be responsible for an increased heat flux in the nanometer-range by using an approximation for the nonlocal reflection coefficients. Loomis and Maris[14] also investigated heat transfer between metallic bodies, showing the influence of the electrical resistivity. Recently, Mulet *et al.*[20,23] showed that the radiative heat transfer between dielectrics supporting surface phonon polaritons is dominated by the surface wave contribution. As a result, the heat flux is monochromatic in this case.

Several experiments have been reported. Tien's collaborators made the first measurements at cryogenic temperatures, when the near field starts at hundreds of microns. Kuteladze and Bal'tsevitch[10] performed an analogous experiment. Hargreaves[6] was the first one to note (at ambient temperature) an enhanced heat transfer over micrometric distances by using two parallel plates of chromium. At the end of the 1980s, Xu and co-workers[12,13] could not confirm this effect with an indium needle in front of silver. Recently, Kittel and co-workers[17,27] showed a large increase in the heat exchange between a scanning probe microscope metallic tip and a planar surface by working in the nanometer range. Surprisingly, they also found that the increase of the heat flux levels off (saturates) at very small scales (a few tens of nanometers). This is in striking contrast with the $1/d^3$ dependence to the distance d of the density of states close to the surface. It is also in contrast with the power laws discussed by Pan.[18] This led Kittel *et al.* to suggest that the observed saturation at short distances could be due to a nonlocal dielectric constant. Very recently, Narayanaswamy[30] measured an enhancement of the heat flux at micron distances using a dielectric polar material and a setup similar to the one used for measurements of the Casimir force.[29] Simultaneously, a number of groups tried to use proximity-enhanced heat transfer to increase locally the number of electric charge carriers. Di Matteo *et al.*[31] reported an experimental observation in 2001. A number of theoretical papers also present heat flux levels.[31–38] It has also been predicted that metamaterials,[24] electron doping,[25] or adsorbates[39] may enhance the near-field heat transfer.

Although the enhancement of the flux becomes very large at distances on the order of a few nanometers, most of the published results use a local model of the dielectric constant. It has been pointed out that nonlocal effects should affect significantly the lifetime of a molecule close to a surface.[40–43] This effect has also been studied in the context of the Casimir force.[44,45] It appears to be a relatively minor correction. The experimental findings of Kittel *et al.* have revived the interest for nonlocal effects as the saturation observed at short distance is a very significant effect. This paper is devoted to the analysis of two questions: (i) What is the origin of the saturation of the flux in the near field? (ii) What are the consequences of nonlocality in the context of near-field radiative heat transfer?

In this paper, we focus on the heat flux between two parallel semi-infinite metallic substrates. We show that for a metal, the *s*-polarized [transverse electric (TE)] contribution is the leading one in the nanometric regime when using local optics. Indeed, the contribution of the familiar $1/d^2$ divergence at short distances due to *p*-polarized waves becomes the leading contribution only below 0.1 nm. The saturation

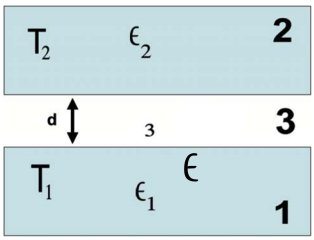

FIG. 1. (Color online) Schematic of the two semi-infinite media with a gap.

of the *s*-polarized contribution is similar to the experimental behavior reported by Kittel *et al.*,[27] so that nonlocal corrections do not seem necessary. To further investigate this issue, we compute the near-field radiative heat transfer using two nonlocal models: the Lindhard-Mermin model based on the random phase approximation and its approximation in the Boltzmann-Mermin model. Both longitudinal and transverse nonlocal dielectric constants are included. We find that a local calculation agrees well with the nonlocal ones at gap distances larger than 2 nm. We finally discuss the physical mechanism responsible for the saturation. We show that it is due to the magnetic fields that generate eddy currents.

II. NEAR-FIELD RADIATIVE HEAT FLUX USING A LOCAL DIELECTRIC CONSTANT

We start the section by summarizing the derivation of the heat flux between two parallel semi-infinite bulks (see Fig. 1). We do not consider any roughness or tilt between the surfaces. Both semi-infinite media are assumed to be in local thermodynamic equilibrium with temperatures T_1 and T_2. This allows to derive the energy radiated by random currents in medium 1 at temperature T_1 and absorbed in medium 2 and vice versa. The model can be extended to inhomogeneous temperature profiles provided that the temperature variation across a distance of the order of the skin depth is negligible. The flux per unit area is given by the normal component of the Poynting vector,

$$\phi = \langle \mathbf{E}(r,t) \times \mathbf{H}(r,t) \rangle \cdot \mathbf{e}_z, \tag{1}$$

where the position r can be taken at the center of the gap $z=0$ and $\langle \cdots \rangle$ denotes a statistical average. Derivations can be found in many articles[8,11,14–16,19,23,46] and will not be repeated here. The final form of the heat flux is

$$\phi = \int_{\omega=0}^{+\infty} d\omega [I_\omega^0(T_1) - I_\omega^0(T_2)] \times \sum_{\alpha=s,p} \left[\int_0^{\omega/c} \frac{KdK}{\omega^2/c^2} \frac{(1-|r_{31}^\alpha|^2)(1-|r_{32}^\alpha|^2)}{|1-r_{31}^s r_{32}^\alpha e^{2i\gamma_3 d}|^2} + \int_{\omega/c}^{\infty} \frac{KdK}{\omega^2/c^2} \frac{4\,\mathrm{Im}(r_{31}^\alpha)\mathrm{Im}(r_{32}^\alpha)e^{-2\gamma_3'' d}}{|1-r_{31}^\alpha r_{32}^\alpha e^{-2\gamma_3'' d}|^2} \right], \tag{2}$$

where d is the distance between the two interfaces, r_{3m} the reflection factor at the interface between medium m and vacuum (medium 3) for a wave with wave vector K parallel to the surface, and polarization $\alpha = s, p$. The wave vector

$$\gamma_m = \sqrt{\epsilon_m \omega^2/c^2 - K^2} = \gamma_m' + i\gamma_m'' \tag{3}$$

describes the propagation across medium m, c is the speed of light, and

$$I_\omega^0 = \frac{\omega^2}{4\pi^3 c^2} \frac{\hbar\omega}{(e^{\hbar\omega/k_B T} - 1)} \tag{4}$$

is the monochromatic specific intensity of blackbody radiation with $\hbar$ and k_B the Planck and Boltzmann constants. We now discuss Eq. (3), which contains an integration over the (K, ω) plane. This equation naturally displays a splitting of the heat flux into *s*- and *p*-polarized waves and into propagating $(K < \omega/c)$ and evanescent waves $(K > \omega/c)$. The denominators account for multiple reflections through a Fabry-Pérot term, $1 - r_{31}^\alpha r_{32}^\alpha e^{-2\gamma_3'' d}$. The Planck function I_ω^0 acts as a temperature-dependent frequency filter that cuts off frequencies much larger than $k_B T/\hbar$, i.e., beyond the near infrared at room temperature. As $\gamma_3'' \simeq K$ for large K parallel wave vectors (deeply evanescent waves), there is also a wave vector filter $(e^{-2\gamma_3'' d})$; wave vectors much larger than $1/2d$ do not contribute to the heat transfer at small gap sizes. This also implies that at submicron distances $d \ll \lambda_T$, the evanescent contribution is much larger than the propagating one, leading to an enhanced heat flux.

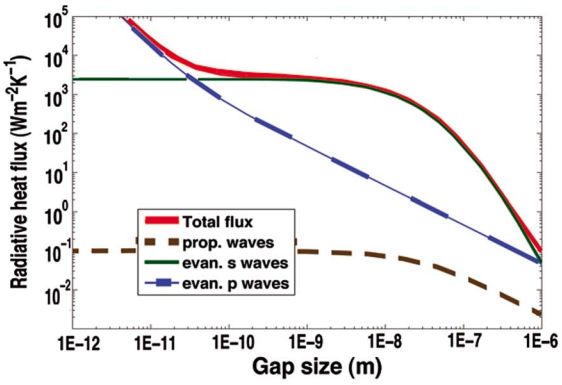

FIG. 2. (Color online) Heat flux per unit area for gold.

In Fig. 2, we show results obtained using a local dielectric constant. We consider a nonmagnetic metallic medium characterized by a Drude model, $\epsilon_{1,2}(\omega) = \epsilon_b - \omega_p^2/(\omega^2 + i\omega\nu)$ where ϵ_b accounts for the bound electron contribution, ω_p is the plasma frequency, and ν is the damping coefficient. This model is appropriate for frequencies up to the infrared range where the metallic response is mainly due to the conduction electrons. In this paper, we present results either for gold ($\epsilon_b = 1$, $\omega_p = 1.71 \times 10^{16}$ s^{-1}, $\nu = 4.05 \times 10^{13}$ s^{-1}) or for aluminum [$\epsilon_b = 2$, $\omega_p = 2.24 \times 10^{16}$ s^{-1}, $\nu = 1.22 \times 10^{14}$ s^{-1}, and we use in Sec. III $v_F = c/148$ where v_F is the Fermi velocity and c is the light velocity].

Figure 2 demonstrates that the increase of the heat flux levels off below distances of 10–30 nm, as was found in previous papers by Polder and Van Hove,[8] Loomis and Maris,[14] and Volokitin and Persson.[19] The saturation is due to a strong *s*-polarized contribution. Only for distances below

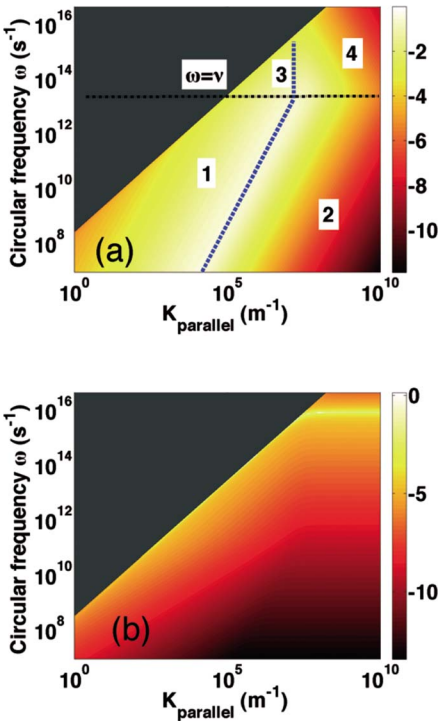

FIG. 3. (Color online) (a) Imaginary part of the s (TE) reflection coefficient for gold. The color bar indicates the order of magnitude (logarithmic scale). The diagonal line (light cone) is the limit between the nonplotted propagative waves $K<\frac{\omega}{c}$ and the evanescent waves $\left(K>\frac{\omega}{c}\right)$. The black dotted line gives the frequency $\omega=\nu$ and the blue dotted lines give the limits between the contributing domain and the one of very large K. (b) Imaginary part of the p (TM) reflection coefficient for gold. The color bar scales the order of magnitude (logarithmic scale). The plasmon resonance occurs near $\omega_{sp}=\omega_p/\sqrt{2}\approx 1.2\times 10^{16}$ s^{-1}.

0.1 nm is the flux dominated by p-polarized waves, but in this regime, the local model is no longer valid (see Fig. 5 below). We note that in practice, with distances in the nanometer range, the s-polarized contribution dominates the heat flux.

We now discuss the behavior of the reflection coefficients in the (K,ω) plane (see Fig. 3). This points to the origin of the leading s-wave contribution. We plot the imaginary part of the reflection factors that is proportional to the heat flux [Eq. (3)]. In particular, also the local density of electromagnetic states (LDOS) is controlled by the imaginary part of the reflection amplitudes, as discussed in Refs. 16 and 56.

First of all, we observe that $\mathrm{Im}\, r_s(K,\omega)$ covers a larger domain in the (K,ω) plane and takes larger values than its p-polarized counterpart. For the latter reflection coefficient, one has the following at large K:

$$\mathrm{Im}\, r_p^{31} \simeq \frac{\omega\nu\omega_{sp}^2(R+1)}{(\omega_{sp}^2-\omega^2)^2+\omega^2\nu^2}+\mathcal{O}[(\omega\sqrt{\epsilon_1}/cK)^2], \qquad (5)$$

where $R=(\epsilon_b-\epsilon_3)/(\epsilon_b+\epsilon_3)$ and $\omega_{sp}^2=\omega_p^2/(\epsilon_b+\epsilon_3)$. If medium 3 is vacuum and the background polarization is negligible, $R=0$, and the surface plasmon-polariton resonance occurs at $\omega_{sp}=\omega_p/\sqrt{2}$. This resonance implies a peak in the near-field radiation spectrum[46] as seen in Fig. 3. For typical metals, it lies in the UV, way above the frequency range that contributes significantly to the heat flux. Note that the asymptotics in Eq. (5) becomes relevant only for extremely large K vectors where $K\gg\omega\sqrt{\epsilon_1}/c\gg\omega/c$; this is why the p polarization becomes dominant only at very short distances (see Fig. 2). For the s polarization, we have the following in the same range of K:

$$\mathrm{Im}\, r_s^{31} \simeq \frac{\omega^2/c^2}{4K^2}\frac{\omega_p^2\nu}{\omega(\omega^2+\nu^2)}+\mathcal{O}[(\omega\sqrt{\epsilon_1}/cK)^4], \qquad (6)$$

which tends to zero like $1/K^2$. This is the reason why the s-polarized contribution is often discarded when looking at the asymptotic behavior.[41] However, as shown in Fig. 3(a), there is a region where $\mathrm{Im}(r_s)$ has large values before decaying, corresponding to the wide interval $\omega/c\ll K\ll\sqrt{|\epsilon_1|}\omega/c$. We detail in the Appendix the behavior of the reflection coefficient and how to find the borders of the regions sketched in Fig. 3(a). The result is an upper wave vector given by

$$K_{\max}\approx\frac{\omega_p}{c}. \qquad (7)$$

Thus, we predict a saturation of the s-polarized heat transfer at gap distances smaller than

$$d_{min}=\frac{c}{\omega_p}=\frac{\delta(\omega\gg\nu)}{\sqrt{2}}, \qquad (8)$$

where the metal skin depth δ is defined by $1/\delta(\omega)=(\omega/c)\mathrm{Im}\sqrt{\epsilon}$. For frequencies between ν and ω_p, $\delta\simeq c/\omega_p$. For gold, the skin depth in this region is $\delta=\sqrt{2}c/\omega_p\approx 25$ nm. It follows that the saturation distance is given by the skin depth at frequencies higher than ν. We note that for gold, $d_{min}\simeq 18$ nm. This is of the same order of magnitude as the cutoff distance in the experiment of Kittel *et al.*[27] and, incidentally, also comparable to the electron mean free path. To summarize this section, we have found that the derivation of the heat flux between two metallic surfaces using a local dielectric constant predicts a saturation of the flux at a distance given by the skin depth.

III. NEAR-FIELD RADIATIVE HEAT FLUX USING A NONLOCAL MODEL

We now turn to a nonlocal description of the heat transfer. There are several reasons to investigate the role of nonlocal effects in the heat transfer. First of all, nonlocal effects become significant at short distances. It has been shown that nonlocality can explain the anomalous skin effect[47] and has a very important effect on the lifetime of an excited atom or particle near a surface.[41–43] It has been seen that it has a significant impact in the problem of near-field friction.[48] It has also been suggested that saturation of the heat flux could be due to nonlocal effects.[27] In addition, it is desirable to analyze the interplay between the skin depth found above and the mean free path.

Temporal dispersion (i.e., frequency dependence of optical properties) appears when the electromagnetic (EM) field

varies on a time scale comparable to the microscopic time scales of the medium where it propagates. A nonlocal behavior (i.e., spatial dispersion or k dependence of the optical properties) is expected if the EM field varies appreciably on length scales given by the microscopic structure of the medium.

For metals, there are several microscopic length scales related to the Fermi velocity v_F of the conduction electrons. The first one is the electron mean free path v_F/ν, typically 20 nm for gold at ambient temperature in the bulk. The second one is the charge screening length in a plasma of electrons called the Thomas-Fermi length, on the order of v_F/ω_p. The third length is the Fermi wavelength $1/k_F=\hbar/m*v_F$ (where $m*$ is the effective mass of the electron). It sets a lower limit for the spatial variations of the electron density in the metal and is often comparable to the Thomas-Fermi length. The fourth characteristic length is the distance v_F/ω traveled by an electron during one period of an applied EM field. This length governs an enhanced absorption by evanescent waves with $K>\omega/v_F$. This process is called Landau damping and consists in the creation of electron-hole pairs by absorption of photons.

In order to account for the bulk effects, we use two different dielectric functions: the Lindhard-Mermin (LM) and the Boltzmann-Mermin (BM) formulas.[41] The LM dielectric function is also known, e.g., as the random phase approximation (RPA),[41] Kliewer-Fuchs,[49] constants, or jellium ones. Other types of nonlocal dielectric functions are possible: the hydrodynamic model is an approximation at small wave number;[50] Feibelman's model[51] focuses on surface effects and has difficulties in taking bulk absorption into account, which plays a significant role in heat transfer. We follow the notations of Ford and Weber for the longitudinal and transverse dielectric functions:[41]

$$\epsilon_l^{LM}(k,\omega)=\epsilon_b+\frac{3\omega_p^2}{(\omega+i\nu)}\frac{u^2 f_l(z,u)}{\left[\omega+i\nu\dfrac{f_l(z,u)}{f_l(z,0)}\right]}, \tag{9}$$

$$\epsilon_t^{LM}(k,\omega)=\epsilon_b-\frac{\omega_p^2}{\omega^2(\omega+i\nu)}\{\omega[f_t(z,u)-3z^2 f_l(z,u)] + i\nu[f_t(z,0)-3z^2 f_l(z,0)]\}, \tag{10}$$

where ϵ_b is the bulk contribution to the dielectric constant. It describes the interband contributions and it is constant in the following as these transitions do not play any role in the frequency range that we address. The Lindhard functions $f_{l,t}(z,u)$ have arguments $z=k/2k_F$ and $u=(\omega+i\nu)/kv_F$, with k_F the Fermi wave vector, and are given by

$$f_l(z,u)=\frac{1}{2}+\frac{1-(z-u)^2}{8z}\ln\frac{z-u+1}{z-u-1}+\frac{1-(z+u)^2}{8z}\ln\frac{z+u+1}{z+u-1}, \tag{11}$$

$$f_t(z,u)=\frac{3}{8}(z^2+3u^2+1)-3\frac{[1-(z-u)^2]^2}{32z}\ln\frac{z-u+1}{z-u-1}-3\frac{[1-(z+u)^2]}{32z}\ln\frac{z+u+1}{z+u-1}. \tag{12}$$

The limit $u\to 0$ has to be taken with a positive imaginary part so that

$$f_l(z,0)=\frac{1}{2}+\frac{1-z^2}{4z}\ln\left|\frac{z+1}{z-1}\right| \tag{13}$$

and

$$f_t(z,0)=\frac{3}{8}(z^2+1)-3\frac{(1-z^2)^2}{16z}\ln\left|\frac{z+1}{z-1}\right|. \tag{14}$$

A semiclassical approximation of these formulas is obtained for wave vectors k much smaller than k_F, taking $z=0$. This gives the Boltzmann-Mermin formulas

$$\epsilon_l^{BM}(k,\omega)=\epsilon_b+\frac{3\omega_p^2}{(\omega+i\nu)}\frac{u^2 f_l(0,u)}{[\omega+i\nu f_l(0,u)]}, \tag{15}$$

$$\epsilon_t^{BM}(k,\omega)=\epsilon_b-\frac{\omega_p^2}{\omega^2(\omega+i\nu)}f_t(0,u), \tag{16}$$

where

$$f_l(0,u)=1-\frac{u}{2}\ln\frac{u+1}{u-1} \tag{17}$$

and

$$f_t(0,u)=\frac{3}{2}u^2-\frac{3}{4}u(u^2-1)\ln\frac{u+1}{u-1}. \tag{18}$$

A few remarks are in order here. First, the Drude formula is recovered at small k (large u and small z). Second, the variable u compares k to a combination of the mean free path v_F/ν and the distance covered by an electron during a period of the field v_F/ω, which can be considered as an "effective mean free path."[52] Third, at very large wave vectors, the logarithms in Eqs. (17) and (18) describe Landau damping. Indeed, even for $\nu=0$, they imply $\mathrm{Im}(\epsilon)>0$ for $k>\omega/v_F$.[43] Finally, it is seen that at very large wave vectors, there is a sharp cutoff in the imaginary parts of the Lindhard-Mermin dielectric functions:

$$\epsilon_t^{LM}(k\gg k_F)=\epsilon_b+\frac{8}{5}\frac{\omega_p^2}{\omega^2}\frac{k_F^2}{k^2}+i\nu\frac{4}{\omega}\frac{\omega_p^2}{v_F^2}\frac{k_F^2}{k^4}, \tag{19}$$

$$\epsilon_l^{LM}(k\gg k_F)=\epsilon_b+\frac{4\omega_p^2}{v_F^2}\frac{k_F^2}{k^4}+i\nu\frac{16\omega\omega_p^2}{v_F^4}\frac{k_F^4}{k^8}. \tag{20}$$

Thus, fields oscillating with spatial periods smaller than half the Fermi wavelength cannot be screened by the electron plasma.

We now account for microscopic surface effects that modify the reflection amplitudes. For the sake of simplicity, we use the infinite barrier model (also known as SCIB), which considers that electrons undergo specular reflection at

the boundary.[41] A model considering diffuse reflection of electrons is also available.[53] In our specular case, the reflection coefficients are computed in terms of surface impedances as follows:

$$r_p^{31} = \frac{\gamma_3/(\omega\epsilon_3) - Z_p}{\gamma_3/(\omega\epsilon_3) + Z_p}, \tag{21}$$

$$r_s^{31} = \frac{Z_s - \omega/(c^2\gamma_3)}{Z_s + \omega/(c^2\gamma_3)}, \tag{22}$$

with

$$Z_s(\mathbf{K},\omega) = \frac{1}{c}\frac{(\mathbf{z}\times\mathbf{K})\cdot\mathbf{E}_1}{\mathbf{K}\cdot\mathbf{B}_1} = \frac{2i}{\pi\omega}\int_0^\infty dq_z \frac{1}{\epsilon_t(k,\omega) - (ck/\omega)^2}, \tag{23}$$

$$Z_p(\mathbf{K},\omega) = \frac{-1}{c}\frac{\mathbf{K}\cdot\mathbf{E}_1}{(z\times K)\cdot\mathbf{B}_1} = \frac{2i}{\pi\omega}\int \frac{dq_z}{k^2}\left(\frac{q_z^2}{\epsilon_t(k,\omega) - (ck/\omega)^2} + \frac{K^2}{\epsilon_l(k,\omega)}\right), \tag{24}$$

where under the integral, $k^2 = K^2 + q_z^2$. $\mathbf{K}$ is the unit vector in the direction of the parallel wave vector K. As we account for spatial dispersion by using a nonlocal model, the reflection coefficients depend on ω and K in a more complicated way than the Fresnel formulas.

One should note that in this approach, we do not tackle several effects that occur on the atomic (subnanometer) scale. The electron density, which is modified near the interface, is treated here with a step form and the addition of surface currents.[41,49] Several authors[41,51] showed that a self-consistent calculation leads to a continuous variation of the electron density between the bulk density and vacuum and that this can be described by an effective mean displacement of the surface, of the order of a few angstroms. Phenomena such as electron tunneling also occur as the two surfaces approach each other on this scale and mutually influence their electron density profiles. We do not take this tunneling into account as it is clearly negligible in the nanometer range.

In Fig. 4(a), we show the imaginary part of r_p at fixed ω. It is related to the local density of states (LDOS) (see Sec. IV). An interesting finding is that the local description leads to a plateau for large K (nonretarded approximation) that does not agree for any value of K with the nonlocal model. The local quasistatic approximation that has been often used thus yields an incorrect value of $\mathrm{Im}(r_p)$ for a very broad range of frequencies. The curve labeled "longitudinal quasistatic" is based on neglecting the first term in Eq. (25), involving the transverse part of the dielectric function. We see that this term nevertheless contributes at wave vectors $K < 1/\delta(\omega) \approx 10^8$ m^{-1}. For larger K, the nonlocal calculation leads to an increase of Im r_p by roughly one order of magnitude, which we attribute to Landau damping. Finally, we

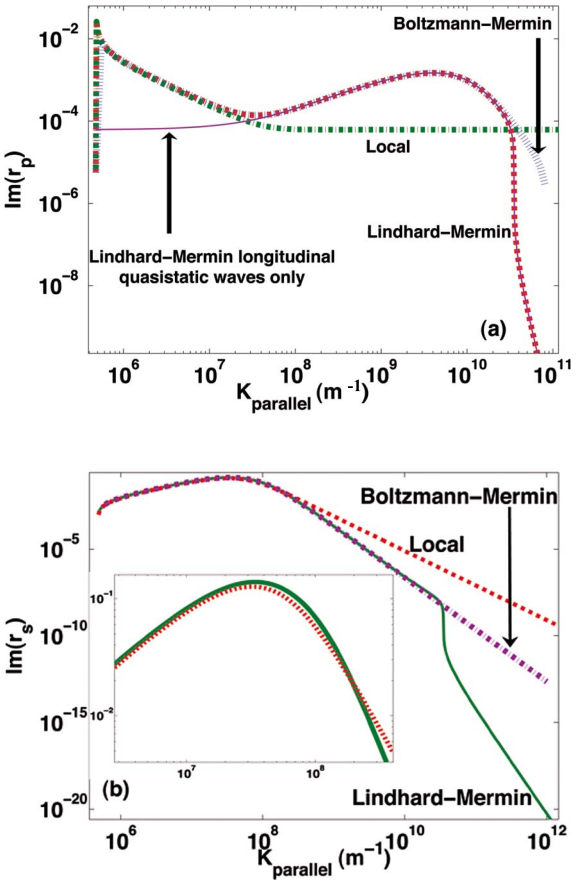

FIG. 4. (Color online) (a) Imaginary part of the p (TM) reflection factor for aluminum for $\omega = 1.4\times10^{14}$ s^{-1}. (b) Imaginary part of the s (TE) reflection factor for aluminum for $\omega = 1.4\times10^{14}$ s^{-1}.

observe that for wave vectors larger than $k_F \approx 10^{10}$ m^{-1}, the nonlocal models predict a strong decay of $\mathrm{Im}(r_p)$ as compared to the local model.

The s-polarized reflection coefficient $\mathrm{Im}(r_s)$ is plotted in Fig. 4(b). Differences to the local calculation are barely visible in the domain $K < 5\times10^8$ m^{-1} where $\mathrm{Im}(r_s)$ takes significant values and contributes to the heat transfer. We thus expect only small corrections to heat transfer from the nonlocal models.

Figure 5 presents the heat flux as a function of the gap distance. We display the fluxes due to s and p polarizations when using both a local and the two nonlocal models introduced above. Although the validity of the models is questionable for distances smaller than 1 nm, we display the flux at smaller distances in order to analyze their physical content when $d \to 0$. What is important here is that the local and nonlocal heat fluxes are identical up to distances on the order of the Thomas-Fermi length v_F/ω_p. It appears that the small modifications of $\mathrm{Im}(r_s)$ give the same final result after integration over K and ω. A small increase of the heat flux[19] due to the onset of Landau damping is observed in the p-polarized contribution but in a regime where s waves dominate and level off. Another observation is that the two nonlocal models are superimposed, showing that the Thomas-Fermi length is sufficient to describe the large K decay of the dielectric constant. Finally, at very short dis-

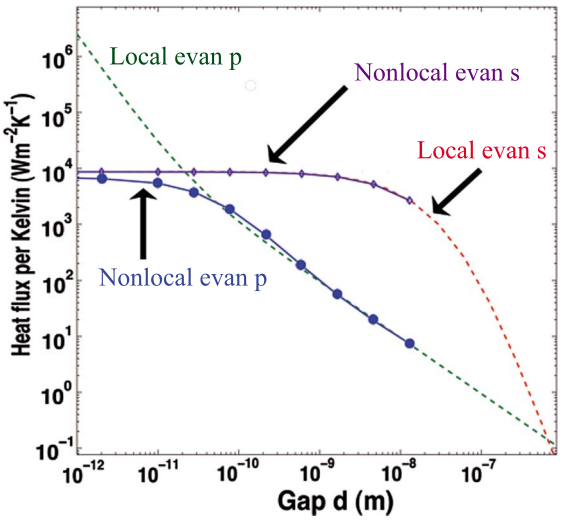

FIG. 5. (Color online) Radiative heat flux between two parallel surfaces of aluminum. The Boltzmann-Mermin and Lindhard-Mermin nonlocal calculations are superimposed. The dotted lines are the local s (red) and p (green) results; the plain lines are the nonlocal s (violet) and p (blue) results.

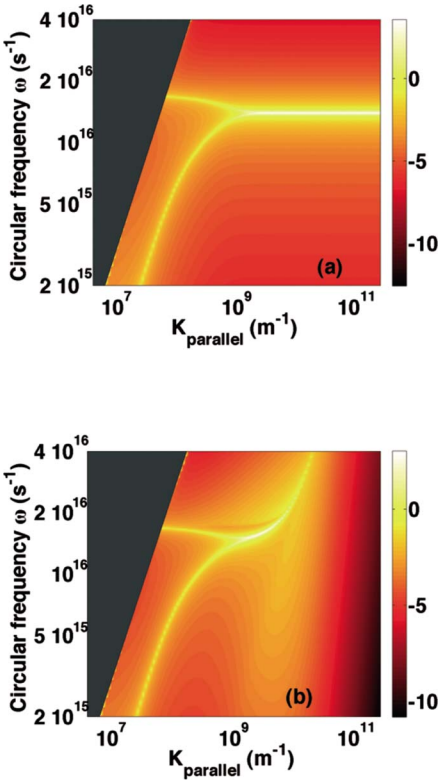

FIG. 6. (Color online) Plot of the expression $\mathrm{Im}(r_p^{31})^2/|1-r_p^2 e^{-2\gamma_3'' d}|^2$ that appears in the integrand [Eq. (3)] of the heat flux for evanescent waves ($K>\omega/c$). The gap size is 2 nm here. The color bar is in logarithmic scale. (a) Local model. (b) Nonlocal Boltzmann-Mermin model. A Lindhard-Mermin model would cut more strongly the integrand at large parallel wave vectors.

tances (below the Thomas-Fermi length or the Fermi wavelength), the nonlocal models remove the $1/d^2$ regime of the p-polarized flux.

We now illustrate how the nonlocal models suppress this $1/d^2$ dependence. In Fig. 6, we have plotted the p-polarized contribution to the heat flux in the (K,ω) plane but removing the decay term $e^{-2\,\mathrm{Im}(\gamma_3)}$ and the Planck function $I_\omega^0(T)$, which act as filters. What we plot is thus $\mathrm{Im}(r_p^{31})^2/|1-(r_p^{31})^2 e^{-2\gamma_3'' d}|^2$. Figure 6 shows a locus that follows the dispersion relation of the surface plasmon polariton. It is seen that it has two branches.[45,54] They split at a wave vector of order $1/d$ that is pushed toward large K as the gap size is decreased. When nonlocality is included, the flat asymptote at frequency $\omega_{sp}=\omega_p/\sqrt{2}$ for large values of K becomes dispersive and approaches $\omega=v_F K$ in Fig. 6(b). However, what is important here is that the far IR branch of the resonance cannot be shifted to the large K region when the gap size decreases because of the cutoff at $\omega=v_F K$. This removes the divergence of the heat flux due to the p-polarized evanescent contribution in Eq. (3) when $d\to 0$. It provides an intrinsic cutoff at large K that is different from the distance d.

The main conclusion of this section is that the local calculation is in practice sufficient when computing heat fluxes between two metallic surfaces a few nanometers apart. The second conclusion is that nonlocality removes the universal heat flux divergence at short distance as expected.

IV. DISCUSSION AND CONCLUDING REMARKS

In this last section, we try to gain some insight on the physical mechanisms responsible for the near-field heat transfer in s polarization between two parallel interfaces. In Fig. 7, we have plotted the LDOS (Refs. 46 and 55) near a metallic-vacuum interface in vacuum. We recall that the local density of energy is the product of the LDOS by the mean energy of an oscillator given by $\hbar\omega/(e^{\hbar\omega/k_B T}-1)$. The LDOS is split into four contributions: magnetic and electric fields

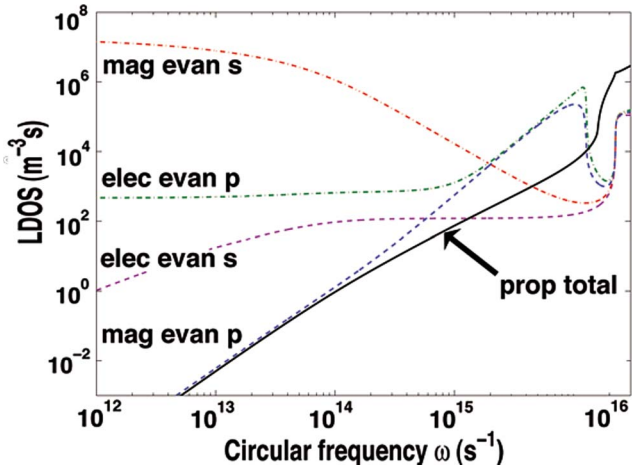

FIG. 7. (Color online) Local density of states near an aluminum interface, calculated with local optics at a distance $d=30$ nm from the surface.

and s and p polarizations. For instance, the contribution of the evanescent s-polarized magnetic field to the LDOS is given by

$$\rho_s^M(z,\omega) = \rho_v \int_{\omega/c}^{+\infty} \frac{dK}{2|\gamma_3|} \frac{cK}{\omega} f(K,\omega) \mathrm{Im}(r_s) e^{-2\gamma_3'' z}, \quad (25)$$

where $\rho_v(\omega) = \omega^2/\pi^2 c^3$ is the vacuum density of states and $f(K,\omega) = 2(\frac{cK}{\omega})^2 - 1$. Again, the properties of the material control the LDOS via $\mathrm{Im}(r_s)$. Figure 7 shows that the propagating terms are negligible. Furthermore, the leading contribution in the infrared ($\omega \approx 10^{13} - 10^{15}$ s^{-1}, where the room-temperature thermal spectrum peaks) is clearly due to s-polarized magnetic fields. It follows that a metallic half-space generates a very large magnetic energy in a vacuum close to the surface. This quantity is relevant to analyze the heat transfer through an interface. Indeed, as the magnetic field is continuous through an interface with a nonmagnetic material, the magnetic field penetrates without reflection.

The large value of the magnetic density of energy due to s-polarized waves near a metallic interface has been discussed recently.[55,56] Whereas the ratio $c|\mathbf{B}|/|\mathbf{E}|$ takes a fixed value of 1 for propagating waves, it becomes frequency-dependent for evanescent waves ($K/k_0 > 1$). For s-polarized evanescent waves, using the Maxwell-Faraday equation, one can show that this ratio is given by $\sqrt{f(K,\omega)} \simeq \sqrt{2} K/k_0$. Magnetic fields dominate in s polarization. For p-polarized waves, the opposite trend $|\mathbf{E}|/c|\mathbf{B}| \simeq \sqrt{f(K,\omega)}$ is found, showing that electric fields dominate. If we want to know which of the magnetic s-polarized waves or the electric p-polarized waves give the leading contribution to the LDOS, we have to compare the products $f(K,\omega)\mathrm{Im}(r_s)$ and $f(K,\omega)\mathrm{Im}(r_p)$. As we have seen, the s-polarized reflection coefficient is larger than $\mathrm{Im}(r_p)$ for a metal at infrared frequencies and below, so that, finally, the LDOS is dominated by its s-polarized magnetic component, as seen in Fig. 7.

It follows that retardation plays a key role as observed in Ref. 19. Accordingly, the heat transfer between a metallic nanoparticle and a half-space[16,19,20] must be revisited, accounting for magnetic energy. It will be shown that the magnetic dipole yields the leading contribution.[56]

The large magnetic fields can be traced back to the current density in the material. In s polarization, the electric field $\mathbf{E}$ is tangential to the metallic interface, and therefore continuous. It drives a surface current flowing within the skin depth δ, with an amplitude roughly given by σE. This suggests the following mechanism for the heat transfer between metallic surfaces: Fluctuating currents flowing parallel to the interface within the skin depth in medium 1 generate large magnetic fields at IR frequencies. These fields penetrate into medium 2 and generate large eddy currents which are dissipated by the Joule effect. In other words, radiative heat transfer in the near field is similar to nanoscale induction heating at infrared frequencies.

In Sec. II, we have seen that the skin depth plays a key role.[57] The above argument provides a simple picture for the phenomenon. The skin depth depends on the frequency. We stress that the cutoff distance seen by Kittel *et al.*[27] and that we found above are linked to the skin depth evaluated at the frequencies contributing to the largest parallel wave vectors, ω_ν. For gold, this skin depth is $\delta = \sqrt{2} c/\omega_p \approx 25$ nm. Our analysis leads to a number of predictions that should be measurable. Measurements of the heat transfer such as those reported by Kittel *et al.* should be able to detect the skin depth dependence by changing the metals. As seen in Fig. 8, the plasma frequencies of a number of metals are not very different. They all give (local) cutoff distances in the range of 10–200 nm. The differences should be measurable. A material like cobalt is expected to saturate at larger distances than metals such as copper, gold, or aluminum. Interestingly, cobalt could also be a test-case study for the saturation due to nonlocality as the p-polarized contribution becomes larger than the s-polarized contribution near 1 nm. Another interesting issue is the heat flux between two different metals. We expect a saturation distance governed by the smallest skin depth due to the product $\mathrm{Im}(r_s^{31})\mathrm{Im}(r_s^{32})$ in the heat flux formula.

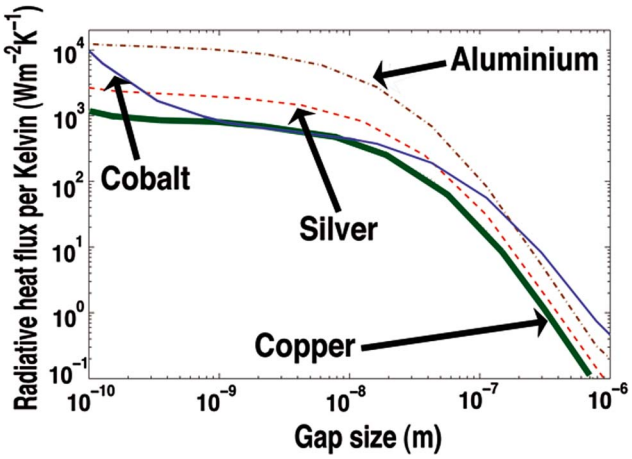

FIG. 8. (Color online) Heat flux per unit area and per Kelvin for different metals.

To summarize, we have shown that the radiative heat flux between two parallel metallic surfaces saturates when the gap size reaches a distance equal to the skin depth at a frequency equal to ν. We have shown that the leading contribution to the flux is due to eddy currents generated in the medium. The nonlocal effects have been studied. They do not significantly affect the s-polarized fields but introduce a cutoff in the K dependence of the p-polarized fields. This cutoff removes the $1/d^2$ dependence of the flux at short distances. As the s-polarized fields dominate the heat transfer between metallic surfaces, the nonlocal corrections are negligible. Finally, we observed that the cutoff distances seem to be in the range of 10–200 nm for many metals.

ACKNOWLEDGMENTS

We thank M. Laroche, M. I. Stockman, and V. B. Svetovoy for useful discussions. We acknowledge the support of the Agence Nationale de la Recherche under Contract No. ANR06-NANO-062-04.

APPENDIX

In this section, we explain how we estimate the limits of the domain in the (K,ω) plane where $\mathrm{Im}(r_s)$ contributes to

the heat flux. As is shown in Fig. 3, the (K,ω) plane can be divided into four areas. Point A is the intersection of the four borders. In all the cases, we consider only evanescent waves: $K \gg k_0$ with $k_0=\omega/c$.

We address first the division of the (K,ω) plane between large K and smaller values. This underlines the different behaviors of regions 1 and 3, on one hand, and regions 2 and 4, on the other hand. The perpendicular wave vector γ_1 is given by

$$K^2 + \gamma_1^2 = \epsilon_1 k_0^2, \tag{A1}$$

where $k_0=\omega/c$. This shows that we have two regimes. To leading order, we have $\gamma_1^2 \simeq -K^2$ at very large K (regions 2 and 4) and $\gamma_1^2 \simeq \epsilon_1 k_0^2$ at smaller K (regions 1 and 3). The transition occurs at a critical wave vector $K^2 \simeq |\epsilon_1 k_0^2|$. This gives a critical wave vector given by

$$K_c(\omega) = \sqrt{|\epsilon_1(\omega)|}k_0 \approx \frac{\omega_p}{c}\sqrt{\frac{\omega}{|\omega + i\nu|}}, \tag{A2}$$

where the last equality applies to the Drude model at frequencies $\omega \ll \omega_p/\sqrt{\epsilon_b}$. Values of r_s in both regimes are now given. To leading order, one finds

$$r_s \approx \begin{cases} -1 - 2\dfrac{iK}{\sqrt{\epsilon_1}k_0} & \text{(regions 1 and 3)} \\ \dfrac{k_0^2}{4K^2}(\epsilon_1 - 1) & \text{(regions 2 and 4).} \end{cases} \tag{A3}$$

At large K, $\mathrm{Im}(r_s)$ decreases to small values that do not contribute significantly to the heat flux integral.

We now address the horizontal division of Fig. 3. The upper region is given by domains 3 and 4 and the lower one by domains 1 and 2. This limit is due to the different behaviors of $\epsilon(\omega)$ if $\omega \ll \nu$ (domains 1 and 2) or $\omega \gg \nu$ (domains 3 and 4). The first two asymptotic orders are

TABLE I. Asymptotic behavior of $\mathrm{Im}(r_s)$. A local Drude model is taken for $\epsilon(\omega)$ with plasma frequency ω_p and relaxation rate ν.

Region	Characteristics	$\mathrm{Im}(r_s)$
1	Far IR, small K	$\dfrac{\sqrt{2\nu}c}{\omega_p}\dfrac{K}{\sqrt{\omega}}$
2	Far IR, large K	$\dfrac{\omega_p^2}{4\nu c^2}\dfrac{\omega}{K^2}$
3	Near IR, small K	$\dfrac{\nu c}{\omega_p}\dfrac{K}{\omega}$
4	Near IR, large K	$\dfrac{\omega_p^2\nu}{c^2}\dfrac{1}{\omega K^2}$

$$\epsilon_1(\omega) \approx \begin{cases} i\omega_p^2/\omega\nu - \dfrac{\omega_p^2}{\nu^2} & \text{(regions 1 and 2)} \\ -\dfrac{\omega_p^2}{\omega^2} + i\dfrac{\omega_p^2\nu}{\omega^3} & \text{(regions 3 and 4).} \end{cases} \tag{A4}$$

The low-frequency expression is also known as the Hagen-Rubens formula. In Table I, we give the corresponding asymptotics for $\mathrm{Im}\, r_s$ in the four regions.

As a function of frequency, the critical wave vector behaves like $K_c \approx (\omega_p/c)(\omega/\nu)^{1/2}$ in the far infrared (small frequencies) and like $K_c \approx \omega_p/c$ for larger frequencies. These two lines cross at $\omega \approx \nu$ which is the point A marked in Fig. 3. At this point, the imaginary part of $r_s(K,\omega)$ reaches its maximum.

According to Eq. (A2), $\mathrm{Im}(r_s)$ takes significant values for K lower than $K_c=\omega_p/c$. This limit yields a saturation length $1/K_c=c/\omega_p$. Note that this length is related to the skin depth as $\delta=\frac{1}{\mathrm{Im}(\sqrt{\epsilon_1}k_0)} \simeq \frac{c}{\sqrt{2}\omega_p}$. At low frequencies (regions 1 and 2), ϵ is purely imaginary, leading to $\delta \simeq \sqrt{2}/K_c$, while in the high-frequency regions 3 and 4, $\delta \simeq 1/K_c$. Hence, at each frequency, the cutoff wave vector is essentially given by the inverse skin depth.

*Electronic address: olivier.chapuis@centraliens.net

[1] S. M. Rytov, Yu. A. Kravtsov, and V. I. Tatarskii, *Principles of Statistical Radiophysics* (Springer, Berlin, 1989), Vol. 3.
[2] E. G. Cravalho, C. L. Tien, and R. P. Caren, J. Heat Transfer **89**, 351 (1967).
[3] A. Olivei, Rev. Phys. Appl. **3**, 225 (1968).
[4] R. P. Caren and C.-K. Liu, in *Progr. Aeronautics and Astronautics 21*, edited by T. J. Bevans (Academic, New York, 1969), p. 509.
[5] E. G. Cravalho, G. A. Domoto, and C. L. Tien, in *Progr. Aeronautics and Astronautics 21*, edited by T. J. Bevans (Academic, New York, 1969), p. 531.
[6] C. M. Hargreaves, Phys. Lett. **30A**, 491 (1969).
[7] G. A. Domoto and C. L. Tien, J. Heat Transfer **92**, 412 (1970).
[8] D. Polder and M. Van Hove, Phys. Rev. B **4**, 3303 (1971).
[9] R. P. Caren, Int. J. Heat Mass Transfer **17**, 755765 (1974).
[10] S. S. Kuteladze and Y. A. Bal'tsevitch, Sov. Phys. Dokl. **8**, 577 (1979).
[11] M. L. Levin, V. G. Polevoi, and S. M. Rytov, Sov. Phys. JETP **52**, 1054 (1981).
[12] K. Dransfeld and J. Xu, J. Microsc. **152**, 35 (1988).
[13] J.-B. Xu, K. Läuger, R. Möller, K. Dransfeld, and I. H. Wilson, J. Appl. Phys. **76**, 7209 (1994).
[14] J. J. Loomis and H. J. Maris, Phys. Rev. B **50**, 18517 (1994).
[15] I. A. Dorofeev, Tech. Phys. Lett. **23**, 109 (1997).
[16] J. B. Pendry, J. Phys.: Condens. Matter **11**, 6621 (1999).
[17] W. Müller-Hirsch, A. Kraft, M. T. Hirsch, J. Parisi, and A. Kittel, J. Vac. Sci. Technol. A **17**, 1205 (1999).
[18] J. L. Pan, Opt. Lett. **25**, 369 (2000). See also A. A. Maradudin, *ibid.* **26**, 479 (2001) and J.-P. Mulet, K. Joulain, R. Carminati, and J.-J. Greffet, *ibid.* **26**, 480 (2001).
[19] A. I. Volokitin and B. N. J. Persson, Phys. Rev. B **63**, 205404 (2001).
[20] J. P. Mulet, K. Joulain, R. Carminati, and J. J. Greffet, Appl. Phys. Lett. **78**, 2931 (2001).

[21] G. V. Dedkov and A. A. Kyasov, Tech. Phys. Lett. **28**, 346 (2002).
[22] C. H. Park, H. A. Haus, and M. S. Weinberg, J. Phys. D **35**, 2857 (2002).
[23] J.-P. Mulet, K. Joulain, R. Carminati, and J.-J. Greffet, Microscale Thermophys. Eng. **6**, 209 (2002).
[24] Z. M. Zhang and C. J. Fu, Appl. Phys. Lett. **80**, 1097 (2002); C. J. Fu, Z. M. Zhang, and D. B. Tanner, J. Heat Transfer **127**, 1046 (2005).
[25] C. J. Fu and Z. M. Zhang, Int. J. Heat Mass Transfer **49**, 1703 (2006).
[26] M. Janowicz, D. Reddig, and M. Holthaus, Phys. Rev. A **68**, 043823 (2003).
[27] A. Kittel, W. Müller-Hirsch, J. Parisi, S. A. Biehs, D. Reddig, and M. Holthaus, Phys. Rev. Lett. **95**, 224301 (2005).
[28] G. Bimonte, Phys. Rev. Lett. **96**, 160401 (2006).
[29] U. Mohideen and A. Roy, Phys. Rev. Lett. **81**, 4549 (1998).
[30] A. Narayanaswamy, Ph.D. thesis, Massachusetts Institute of Technology, 2007.
[31] R. S. DiMatteo, P. Greiff, S. L. Finberg, K. Young-Waithe, H. K. H. Choy, M. M. Masaki, and C. G. Fonstad, Appl. Phys. Lett. **79**, 1894 (2001).
[32] J. E. Raynolds, AIP Conf. Proc. **460**, 49 (1999).
[33] J. L. Pan, H. K. H. Choy, and C. A. Fonstad, Jr., IEEE Trans. Electron Devices **47**, 241 (2000).
[34] P. F. Baldasaro, J. E. Raynolds, G. W. Charache, D. M. DePoy, C. T. Ballinger, T. Donovan, and J. M. Borrego, J. Appl. Phys. **89**, 3319 (2001).
[35] M. D. Whale, IEEE Trans. Energy Convers. **17**, 130 (2001).
[36] A. Narayanaswamy and G. Chen, Appl. Phys. Lett. **82**, 3544 (2003).
[37] R. L. Chen, Report No. AIAA2005-960, 2005 (unpublished).
[38] M. Laroche, R. Carminati, and J.-J. Greffet, J. Appl. Phys. **100**, 063704 (2006).
[39] A. I. Volokitin and B. N. J. Persson, Phys. Rev. B **69**, 045417 (2004).
[40] B. N. J. Persson and N. D. Lang, Phys. Rev. B **26**, 5409 (1982).
[41] G. W. Ford and W. H. Weber, Phys. Rep. **113**, 195 (1984). Note a mistake in formula (2.29) corrected, for example, in Ref. 44.
[42] I. A. Larkin and M. I. Stockman, Nano Lett. **5**, 339 (2005).
[43] I. A. Larkin, M. I. Stockman, M. Achermann, and V. I. Klimov, Phys. Rev. B **69**, 121403(R) (2004).
[44] R. Esquivel and V. B. Svetovoy, Phys. Rev. A **69**, 062102 (2004).
[45] B. E. Sernelius, Phys. Rev. B **71**, 235114 (2005).
[46] K. Joulain, J. P. Mulet, F. Marquier, R. Carminati, and J. J. Greffet, Surf. Sci. Rep. **57**, 59 (2005).
[47] First articles are due to A. B. Pippard, Proc. R. Soc. London, Ser. A **191**, 385 (1947) and G. E. H. Reuter and E. H. Sondheimer, *ibid.* **195**, 336 (1948).
[48] A. I. Volokitin and B. N. J. Persson, Phys. Rev. B **68**, 155420 (2003).
[49] J. Lindhard, K. Dan. Vidensk. Selsk. Mat. Fys. Medd. **28**, 8 (1954); K. L. Kliewer and R. Fuchs, Phys. Rev. **181**, 552 (1969); R. Fuchs and K. L. Kliewer, *ibid.* **185**, 905 (1969). The formulas are corrected in N. D. Mermin, Phys. Rev. B **1**, 2362 (1970) and P. de Andrés, R. Monreal, and F. Flores, *ibid.* **34**, 7365 (1986).
[50] P. Halevi, Phys. Rev. B **51**, 7497 (1995).
[51] P. J. Feibelman, Prog. Surf. Sci. **12**, 287 (1982).
[52] C. Henkel and K. Joulain, Appl. Phys. B: Lasers Opt. **84**, 61 (2006).
[53] V. U. Nazarov, Phys. Rev. B **56**, 2198 (1997).
[54] E. N. Economou, Phys. Rev. **182**, 539 (1969).
[55] K. Joulain, R. Carminati, J. P. Mulet, and J. J. Greffet, Phys. Rev. B **68**, 245405 (2003).
[56] P. O. Chapuis, M. Laroche, S. Volz, and J. J. Greffet, Phys. Rev. B (to be published 15 February 2008).
[57] C. Henkel, K. Joulain, R. Carminati, and J. J. Greffet, Opt. Commun. **183**, 57 (2000).